Millimeter Wave Detection of Localized Anomalies in the Space Shuttle External Fuel Tank Insulating Foam

S. Kharkovsky[1], *Senior Member IEEE*, J.T. Case[1], *Student Member IEEE*, M.A. Abou-Khousa[1], *Student Member IEEE*, R. Zoughi[1], *Senior Member IEEE* and F. Hepburn[2]

[1]Applied Microwave Nondestructive Testing Laboratory (*amntl*)
Electrical and Computer Engineering Department
University of Missouri-Rolla
Rolla, Missouri 65409

[2]NASA Marshall Space Flight Center
Marshall Space Flight Center, AL 35812

Abstract

The Space Shuttle Columbia's catastrophic accident emphasizes the growing need for developing and applying effective, robust and life-cycle oriented nondestructive testing (NDT) methods for inspecting the shuttle external fuel tank spray on foam insulation (SOFI). Millimeter wave NDT techniques were one of the methods chosen for evaluating their potential for inspecting these structures. Several panels with embedded anomalies (mainly voids) were produced and tested for this purpose. Near-field and far-field millimeter wave NDT methods were used for producing images of the anomalies in these panels. This paper presents the results of an investigation for the purpose of detecting localized anomalies in several SOFI panels. To this end, reflectometers at a relatively wide range of frequencies (Ka-band (26.5 – 40 GHz) to W-band (75 – 110 GHz)) and utilizing different types of radiators were employed. The resulting raw images revealed a significant amount of information about the interior of these panels. However, using simple image processing techniques the results were improved in particular as it relate s to detecting the smaller anomalies. This paper presents the results of this investigation and a discussion of these results.

Keywords – millimeter waves, nondestructive testing, Space Shuttle, insulating foam, SOFI.

I. INTRODUCTION

The Space Shuttle Columbia's catastrophic failure has been attributed to a piece of external tank spray on foam insulation (SOFI) striking the leading edge of the left wing of the orbiter causing significant damage to some of the protecting heat tiles [1]. There is an urgent need for an advanced nondestructive testing (NDT) technique capable of inspecting the external tank SOFI during and subsequent to the application of the foam and prior to a launch. Such a comprehensive inspection technique enables NASA to perform *life-cycle* inspection on the external tank and its supporting hardware. Consequently, NASA Marshall Space Flight Center initiated an investigation into several potentially viable NDT techniques for this purpose [2-7]. One such method involves the use of millimeter wave NDT techniques to achieve these goals [2, 5-7]. The results of these investigations, on panels that provided for different and important geometries related to the complex structural properties of the external tank, have clearly pointed to the effective potential utility of millimeter wave NDT techniques for testing the Space Shuttle external tank SOFI [6]. However, to better understand the capabilities and limitations associated with these techniques, there is a need for a systematic investigation into evaluating the capabilities of these techniques for detecting localized anomalies (i.e., voids) of different sizes and at different depths with the SOFI.

This paper presents the results of an investigation for the purpose of detecting localized anomalies in several SOFI panels. To this end, millimeter wave reflectometers operating at a relatively wide range of frequencies (Ka-band (26.5 – 40 GHz) to W-band (75 – 110 GHz)) and utilizing different types of radiators were employed in conjunction with several specially

manufactured SOFI panels. Finally, the results of applying a simple image processing algorithm on the obtained images, for improving the measurement results, are also provided.

II. SAMPLE SPECIFICATION AND MEASUREMENT APPROACH

Millimeter wave NDT methods have been used in a wide range of applications [8]. Signals at millimeter wave frequencies are attractive for inspecting low loss dielectric materials since they can penetrate inside of these materials with relative ease. Moreover, the relatively small wavelengths associated with these signals render high spatial resolution images of the interior of various complex, thick and layered composite structures [8-9]. The Space Shuttle's external fuel tank SOFI is in the family of low permittivity and low loss dielectric materials. The relative dielectric properties of the SOFI was measured at X-band, using a completely-filled rectangular waveguide approach, to be $\varepsilon_r = 1.05 - j0.003$ [2]. This is expected since the foam is primarily composed of small air bubbles contained in a low permittivity and low loss polymer. In addition, the SOFI is a homogeneous material at millimeter wave frequencies due to the small size of the air bubbles compared to the operating wavelengths (i.e., several orders of magnitude smaller). Two different sets of SOFI samples were produced for this investigation in which cylindrical voids with different diameters and heights were milled (i.e., drilled out).

Sample Set #1

The first set of samples consisted of two 300 mm by 300 mm-wide and 75 mm-thick SOFI panels, each adhered to an aluminum substrate. A set of twenty cylindrical voids were milled in (drilled out) each panel. Figure 1a shows the picture of one of these panels, and Fig 1b shows the schematic of the relative locations of the twenty voids and their diameters which ranged

between 3 mm to 25 mm. The height of these voids and their locations above the aluminum substrate (i.e., location within the panel thickness) varied for each panel as shown in Figs. 2a and 2b (designated as panels #1 and #2), respectively. The combination of these panels provided for a geometrically diverse number of embedded voids. It must be noted that although these embedded anomalies mostly took the shape of cylindrical cavities/voids, the ones with relatively small heights actually simulate unbonds and delaminations in SOFI.

Sample Set #2

The second sample set consisted of four 550 mm by 240 mm-wide and 70 mm-thick SOFI slabs. In one of these slabs five cylindrical voids (i.e., flat bottom holes) with the diameter of 25 mm and with heights of very close to 25 mm, 18 mm, 12 mm, 6 mm and 3 mm were milled. The spacing between the centers of any two voids was about 95 mm. Figure 3 shows the side and top schematic view of this panel (Fig. 3a shows the slab on top of an aluminum substrate). Another slab was similarly manufactured except that the void diameters were 6 mm. The other two slabs did not have any voids in them. Consequently, each of the slabs with the five flat bottom holes could be used in conjunction with those devoid of holes to produce testing sample panels in which the height of the voids above an aluminum substrate could be varied using different combinations of the three SOFI slabs. In this way, localization of the voids at different depth from an aluminum substrate could be accommodated. The schematics of the possible combinations that were subsequently used in this investigation are shown in Fig. 4.

Experimental Setup

In this investigation, several laboratory-designed millimeter wave reflectometers were used for producing images of these panels at a relatively wide range of frequencies encompassing Ka-band (26.5 – 40 GHz) to W-band (75 – 110 GHz). Some of these experiments involved the use of radiators such as small horn antennas with the panels primarily placed in their near-field regions, while others consisted of inspecting the panels in the far-field of a focused lens antenna. When a panel is placed in the near-field region of a horn antenna the resulting image possesses a relatively high spatial resolution. This is due to the fact that when operating in the near-field region of a probe/antenna, spatial resolution is primarily a function of the probe size [8]. Focusing lens antennas can produce much smaller footprints (e.g., narrow beamwidths) at their designed focal length (i.e., far-field) [10]. The footprint associated with the lens antennas used in this investigation was 12 mm and 6 mm, respectively. The focal length of these lenses was 254 mm at the operating frequency of 100 GHz.

The SOFI panels were placed on 2D automated scanning tables, while the reflectometers were held at a fixed position above the panels. In this way 2D scans/images of the panels were produced at different frequencies and standoff distances (e.g., the distance between the radiator and the surface of a panel). A dc voltage, proportional to the reflected signal characteristics (i.e., phase or magnitude) from the panel under test was then measured and recorded in a matrix corresponding to the scanning area. Subsequently, the measured voltages in this matrix were normalized (with respect to the highest voltage value) and a greyscale image of the panel was produced.

III. RESULTS

Figures 5a-5c show the images of SOFI panel #1 obtained at frequencies of 33.5 GHz (Ka-band), 70 GHz (V-band) and 100 GHz (W-and) using the near-field approach with a small horn antenna, while Fig. 5d shows the image of this panel at 100 GHz using the lens antenna with the 12 mm-diameter footprint. Dimensions in these images as well as all other images in this paper are in mm. Fig.5a shows the Ka-band images of the voids which are manifested by circular indications. The indication at the bottom right hand corner of the image is that of a void with a diameter of 25 mm and a height of 15 mm placed on the aluminum substrate, while the indication at the top right hand corner is due to a similar void but with a height of 3 mm. As expected, the indication of the former void is stronger than the latter due to the difference between their respective heights. On the other hand, it was unexpected to see that the indications of voids located in the middle of the panel (second and third rows from the top) are stronger than indications of larger voids. The reason for this will be explained later. From Fig.5a it is clear that at least seventeen of the voids are readily detected. The three voids that are not readily detected (the three voids from the top in the left hand column) correspond to the smallest voids in this panel all with diameters of 3 mm and heights of 3 mm, 6 mm and 12 mm, respectively. However, some of these voids were detected at higher frequencies. For instance, the smallest void with diameter of 3 mm and height of 3 mm can be seen in the top right corner of the 70 GHz image of the panel, as shown in Fig.5b. This illustrates the positive effect of the higher spatial resolution at 70 GHz. Moreover, higher frequency reflectometers are capable of detecting voids in the SOFI and other anomalies such as non-uniformities in the adhesive layer between SOFI and the substrate (Figs.5b–5d). The 100 GHz image (Fig. 5c) using a small horn antenna, provides more details about the adhesive layer than the other images, as expected. Figure 5d

shows the image of the panel at 100 GHz using the 12 mm-diameter footprint lens antenna. The results give void dimensions that are close to their actual dimensions. In this case small voids in this panel were not detected either, because of the relatively high sensitivity of the lens antenna to non-uniformities of the adhesive layer which masked these small voids. The curvy features in these images (Figs. 5b-5d) are associated with the non-uniformities of the adhesive layer. The presence of this non-uniformity is also the reason why some of the voids whose locations coincided with it had stronger indications in Fig. 5a (i.e., constructive interference).

SOFI panel #2 was scanned using small horn antennas at Ka-band and V-band, as shown in Figs. 6a-6b. In both images the circular indications of the voids are clearly evident similar to panel #1. The indication at the top right hand corner of the image is that of a void with a diameter of 25 mm and a height of 25 mm placed right above the aluminum substrate, while the indication at the bottom right hand corner is that of the void with a diameter of 25 mm and a height of 12 mm located 13 mm above the substrate (see Fig. 2b). As expected, the former indication is much stronger than the latter due to the difference between their respective heights and locations above the substrate. The three voids that are not visible in Fig. 6a (the three voids from the bottom in the left hand column) correspond to the smallest voids with diameters of 3 mm and heights of 12 mm, 6 mm and 3 mm, respectively. These three voids were placed 12 mm, 6 mm and 3 mm above the aluminum substrate, respectively. It should be noted that these voids could be masked by the non-uniformity associated with the adhesive layer which can be seen near their locations in the V-band image (a dark patch in Fig. 6b). Comparison between the 70 GHz images of panels #1 and #2 (Figs. 5b and 6b) shows that the application of the adhesive in panel #2 was more uniform than that in panel #1. Nevertheless, the image of panel #2 indicates non-

uniformities associated with the adhesive layer in the top and bottom right corners of the panel as well as in the area of the two left hand columns in the middle of the panel. Subsequently, the SOFI in panel #2 was cut away at the base from the substrate and placed on a different aluminum substrate without using any adhesive. Figure 7 shows the image of this panel at 70 GHz indicating the absence of the adhesive layer and the non-uniformity that was associated with it before. It is very likely that the smallest voids in this panel were not detected since their heights were significantly reduced as a result of cutting the SOFI.

Figures 5-7 are raw images and no signal/image processing was applied to them. This is significant since they show the effectiveness of these millimeter wave NDT methods for producing rapid and informative images of the interior of SOFI. The results shown in Figs. 5-7 also indicate that these raw images can provide reasonably close estimate of the void diameters. The results also show the ability to closely determine the relative location of a void in an extended SOFI panel. The images shown thus far are the products of the combination of specific antenna radiation patterns and void geometries and dimensions. Therefore, it is possible to use deconvolution algorithms or other image enhancement techniques to remove the effect of antenna radiation pattern from these images resulting a closer size estimate and shape of a void [11-12].

Figures 8 and 9 show images of the 25 mm-diameter and 6 mm-diameter milled voids (i.e., flat bottom hole samples), respectively in the single-slab, double-slab and triple-slab sample combinations, using the lens antenna at 100 GHz. The results in Fig. 8 indicate that the voids with heights of (from left to right) 25 mm, 18 mm, 12 mm and 6 mm were detected at all three

distance combinations above the substrate. The void with the smallest height of 3 mm can be seen on the single- and the triple-slab samples but not in the double-slab sample. One can also see from Fig. 9 that the 6 mm-diameter voids with heights (from left to right) of 25 mm, 20 mm, 10 mm, 5 mm were detected. However, clutter signal due to the small and non-uniform thickness gaps present in between different slabs resulted in masking out some of the voids. In practice such artificial gaps do not exist and therefore this is not to be considered as a limitation when using this technique. Nevertheless, in this investigation the presence of these gaps caused some masking of the desired signals from the voids.

It is important to note that lens antenna with smaller focusing footprints produce images that have higher spatial resolutions which is the direct consequence of higher overall sensitivity to the presence of an anomaly. This fact is demonstrated by using the lens antenna with the smaller 6 mm-diameter footprint in conjunction with this sample set. Figure 10 shows the image of the triple-slab case when the voids are located at the substrate using this lens. Comparison of this image with its counterpart using the previous lens (Fig. 8, triple-slab (a)) shows that all five voids are clearly detected, whereas in Fig. 8 the smallest void is not very clearly detected.

It should be noted that the thicknesses of the triple-slab and the double-slab samples were comparable with focal lengths of the lenses used. Consequently, the images shown in Figs. 8 and 9 were obtained at distance between the lens antenna and the voids that was somewhat longer than focal length of the lens which is 254 mm. Additionally, when operating exactly at the focal lengths resulted in measurements that were sensitive to the presence of slight gaps that were mentioned earlier.

It is also important to further discuss the differences associated with the void images in Figs. 8 and 9. As shown Fig. 8, although all the voids were milled with the same diameter, i.e., 25 mm, they do not project the same signature in the captured images. It is evident that as the height of the void decreases, its spatial signature appears to become fainter. This is mainly attributed to two factors. First, voids with larger volumes tend to have higher reflection than the ones with smaller volumes. Consequently, the small voids are more vulnerable to being masked out when in the vicinity of voids of higher volumes. Second, small voids are more susceptible to the presence of clutter (i.e., unwanted noise-like signal due to SOFI inhomogeneity, system noise, etc.). Consequently, by taking these two factors into account, the raw images (Figs. 8 and 9) can be enhanced considerably using simple image processing techniques such as that utilized below.

In order to enhance the captured images, it becomes crucial to estimate the clutter contaminating the raw data. Typically, this clutter appears as a low pass signal with a dc component that possesses a gradient in one direction only which is generally caused by standoff distance variation. Hence, it is sufficient to estimate this background dc component which represents the clutter level and subtract it from the raw data. To retrieve the signature of each void individually, the raw images were segmented, around a given void, after removing the clutter, resulting in each segment being normalized with respect to its local dynamic range. It is important to note that this procedure can be implemented without the need for *a-priori* knowledge of the locations of the voids. This is especially true when the clutter level is relatively accurately estimated and removed, as described above. However, when the estimate of the clutter is biased, such as when the background signal is not very uniform, this technique may

actually increase the clutter level in some cases. In the present study, this situation may occur if there is significant level of material inhomogeneity associated with a region of the SOFI. Consequently, these regions may falsely indicate the presence of a void (i.e., false positive). To reduce the possibility of this from occurring, a threshold filtering followed by low pass filtering is used after the segmented image is normalized with respect to its dynamic range. Basically, each intensity level in the normalized image is compared to a threshold value. Subsequently, all of the intensity levels that are below the threshold are filtered out, and the intensities that are greater than the threshold are preserved in the image. Figure 11 shows the images of the 25 mm-diameter voids after applying the aforementioned technique with the threshold set at 0.35 (where a normalized image contains values from 0 to 1) followed by a 2 by 2 rectangular kernel as the low pass filter. Comparing these images with their raw counterparts (Fig. 8, voids with 25 mm in diameter), it is apparent that the processed images possess higher fidelity. In most cases, the spatial signatures of the voids can be readily retrieved from the processed images. Figure 12 shows the results of this image enhancement technique when applied to the 6 mm-diameter voids. In this case the threshold was set at 0.1 and a 2 by 2 rectangular kernel was used as a low pass filter. Once again a comparison between these images and those shown in Fig. 9 shows the resulting image enhancement especially for the single-slab and the double-slab samples. In the former sample however, this technique enhanced the clutter level as well as the desired signal. This is mainly due to the fact that the reflections from the non-uniformities, e.g., the slight and non-uniform gaps between the slabs, are comparable to those coming from the voids. As mentioned earlier, such an artificially introduced clutter is not expected to be encountered in practice. Thus, it is expected that this technique will perform well in real-life inspection scenarios.

The optimum threshold value can be set based on the desired probability of detection and the tolerable probability of false alarm (i.e., false positive). These probabilities are usually decided based on the reflected signal level, the clutter level, and the number of available realizations of the captured image. For instance, if several independent replicas of the images of the same anomalies (i.e., several voids) are captured results in a higher probability of detection and a lower probability of false alarm. Intuitively, the optimum threshold level is different for different voids and imaging setups. Hence, one can not assume a preset threshold level for all possible images. However, as a rule of thumb a high threshold level is used when the minimum detectable void size is relatively large. On the other hand, when the system is designed to detect smaller voids, lower threshold levels that allow for weaker reflected signals to pass may be utilized.

IV. SUMMARY AND DISCUSSIONS

It is imperatively critical to detect and evaluate the properties of undesired manufactured or in-service produced anomalies such as voids and unbonds in the Space Shuttle's external tank SOFI. Millimeter wave NDT methods have been shown to be viable candidates for *life-cycle* inspection of the SOFI. To this end, the primary objective of this investigation has been to assess the capabilities of these techniques for detecting localized anomalies as a function of their dimensions, location with SOFI thickness and millimeter wave inspection system properties. Several specifically manufactured SOFI panels were used in this investigation with embedded voids with varying diameters, heights and locations within various SOFI panels. Millimeter wave reflectometers at Ka-band (26.5 – 40 GHz), V-band (50 - 75 GHz) and W-band (75 – 110

GHz) were used to inspect these panels. Additionally, small horn and focused lens antennas were used in conjunction with these reflectometers providing for the possibility of near-field and far-field measurements.

The overall results showed that small voids (diameter of 3 mm and height of 3 mm in 70 mm-thickness SOFI and diameter 6 mm and height of 2.5 mm in 140 mm- and 210 mm-thick SOFI) were detected. It was also shown that these anomalies may be detected in a relatively wide range of frequencies within the millimeter wave frequency spectrum. It was also shown that frequency diversity may result in eliminating clutter sources such as the application of non-uniform adhesive. However, in these cases this apparent gain was at a cost of reduction in spatial resolution (Fig. 5). In addition, the utility of small horn antennas as well as more sophisticated focused lens antennas was also demonstrated. Operating in the near-field region of a horn antenna produced informative (both quantitative and quantitative) images. As expected, high resolution images were produced using the focused lens antennas. Small horn antennas seemed to provide better detection of anomalies in a relatively thin SOFI while the focused lens antennas performed much better when inspecting a relatively thick SOFI.

Several panels used in this investigation had thicknesses which were comparable to the focal lengths of the lenses used. Consequently, in these cases the distance between the lens antennas and the voids was somewhat longer than the focal lengths. Nevertheless, small voids right above the substrates as well as small voids at different depths within the SOFI slabs were detected. This is an advantage of using these techniques since multiple voids located at different depths within the SOFI can be simultaneously detected in one scan/image (i.e., no need to change lens

distance to a panel to detect voids at different depths). This fact has also been demonstrated in a previous investigation [7].

The lens with the smaller footprint produced higher spatial resolution images. One must be careful that in this case the small footprint associated with the lens may also contribute to a higher level of clutter produced as a result of small non-uniformities with SOFI. To this end a relatively simple image processing algorithm was successfully implemented to obtain more information about the properties of the embedded voids.

ACKNOWLEDGMENT: Funding for this work was provided by the NASA Marshall Space Flight Center through a Cooperative Agreement.

REFERENCES

1. Columbia Accident Investigation Board Report, NASA, August 2003.
2. Shrestha S., S. Kharkovsky, R. Zoughi, F.L. Hepburn and G. Workman, "Microwave Nondestructive Inspection of Thick Insulating Foam," *The American Society for Non-Destructive Testing (ASNT) Fall Conference and Quality Testing Show*, Pittsburgh, PA, 13-17 October 2003.
3. Davis C., F. Santos, "Shearography NDE of Space Launch Vehicles," *The American Society for Non-Destructive Testing (ASNT) Fall Conference and Quality Testing Show*, Pittsburgh, PA, 13-17 October 2003.
4. Madaras E., "Terahertz NDE for Inspection of Shuttle Foam," *The American Society for Non-Destructive Testing (ASNT) Fall Conference and Quality Testing Show*, Pittsburgh, PA, 13-17 October 2003.
5. Shrestha S., S. Kharkovsky, R. Zoughi, and F.L. Hepburn, "Microwave and Millimeter Wave Nondestructive Evaluation of the External Tank Insulating Foam," *Materials Evaluation*, vol.63, N3, pp.339-344, March 2005.
6. Kharkovsky S., F. Hepburn, J. Walker, R. Zoughi. Nondestructive Testing of the Space Shuttle External Tank Foam Insulation using Near Field and Focused Millimeter Wave Techniques, *Materials Evaluation*, vol. 63, N5, pp. 516-522, 2005.
7. Kharkovsky S., J.T. Case, R. Zoughi and F. Hepburn. Millimeter Wave Detection of Localized Anomalies in the Space Shuttle External Fuel Tank Insulating Foam and Acreage Heat Tiles, *Proc. 22nd IEEE Instrumentation and Measurement Technology Conference*, Ottawa, Canada, pp.1527-1530, 2005.
8. Zoughi, R., *Microwave Non-Destructive Testing and Evaluation*, Kluwer Academic Publishers, The Netherlands, 2000.
9. Bakhtiari, S., S. Ganchev, N. Qaddoumi and R. Zoughi, "Microwave Non-Contact Examination of Disbond and Thickness Variation in Stratified Composite Media," *IEEE Transactions on Microwave Theory and Techniques*, vol. 42, no. 3, pp. 389-395, March, 1994.
10. Balanis, C.A., *Antenna Theory: Analysis and Design*, 2nd Edition, John Wiley and Sons, NY, NY, 1997.
11. Nandi, A.K. and D. Mampel, "Deconvolution of Ultrasonic Signals in Nondestructive Testing Applications," *Proceedings of IEEE Signal Processing/ATHOS Workshop on Higher-Statistics*, Girona, Spain, pp. 243-247, June 1995.
12. Hayward, G. and J.E. Lewis, "Comparison of Some Non-Adaptive Deconvolution Techniques for Resolution Enhancement of Ultrasonic Data", *Ultrasonics*, vol. 27, no. 5, pp. 155-164, 1977.

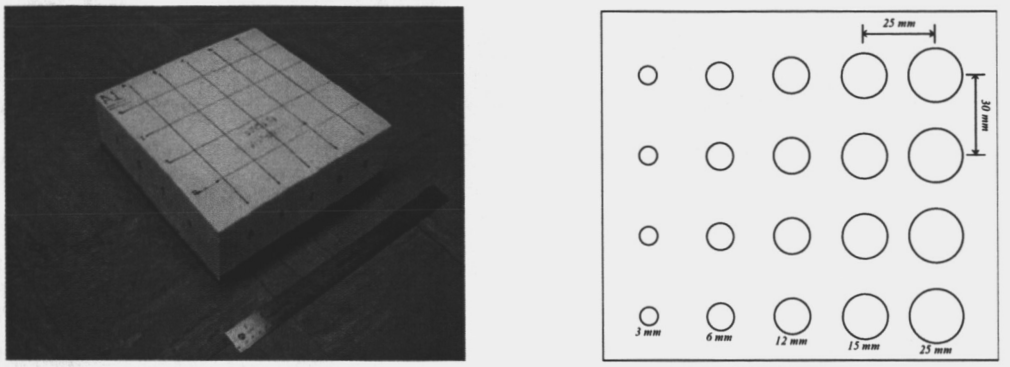

(a) (b)

Figure1: The 75 mm-thick SOFI panel with twenty embedded voids: (a) picture and (b) top view schematic.

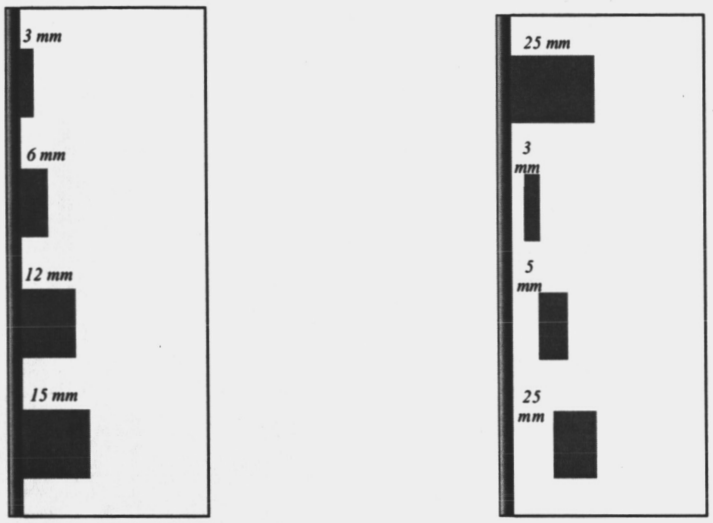

Figure 2: Side view schematic of the 75 mm-thick SOFI: (a) panel #1 and (b) panel #2.

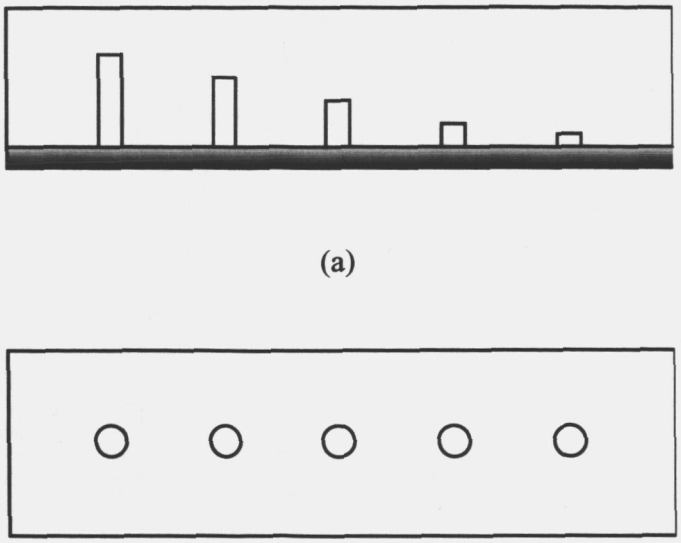

(a)

(b)

Figure 3: (a) Side view and (b) top view schematic of the 70 mm-thick SOFI single-slab panel.

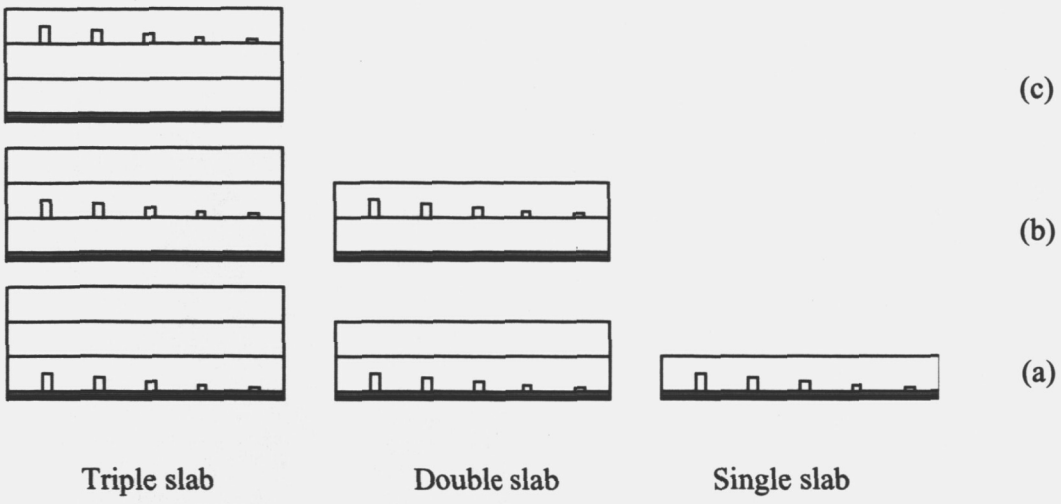

Figure 4: Side view schematic of SOFI panels with voids located at different depths: (a) at substrate, (b) 70 mm from substrate and (c) 140 mm from substrate.

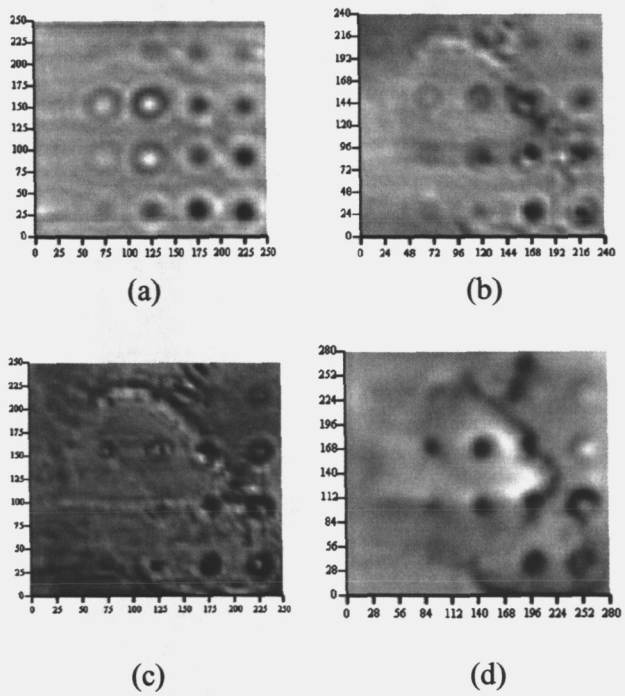

Figure 5: Millimeter wave image of panel #1: (a) 33.5 GHz using a horn antenna; (b) 70 GHz using a horn antenna; (c) 100 GHz using a horn antenna and (d) 100 GHz using the 12 mm-diameter footprint lens antenna.

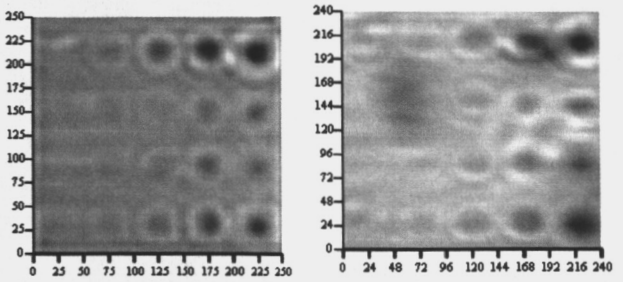

(a) (b)

Figure 6: Millimeter wave image of SOFI panel #2 using a small horn antenna at: (a) 33.5 GHz and (b) 70 GHz.

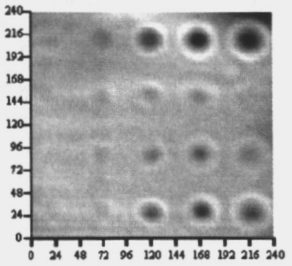

Figure 7: 70 GHz image of SOFI panel #2 without adhesive between foam and aluminum substrate.

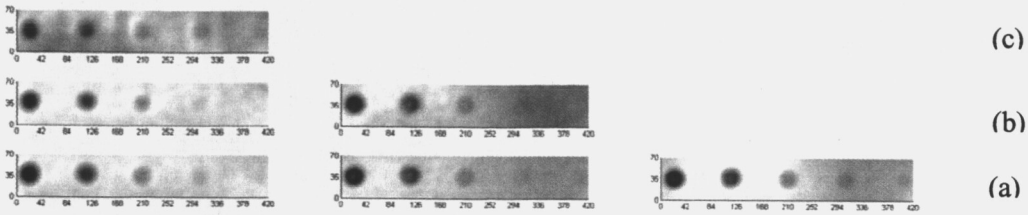

Figure 8: 100 GHz images of 25 mm-diameter milled voids with different heights located in SOFI panels at different depths: (a) at substrate, (b) 70 mm from substrate and (c) 140 mm from substrate.

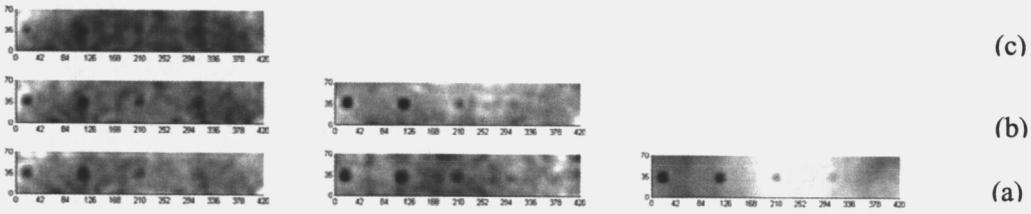

Figure 9: 100 GHz images of 6 mm-diameter milled voids with different heights located in SOFI panels at different depths: (a) at substrate, (b) 70 mm from substrate and (c) 140 mm from substrate.

Figure 10: 100 GHz images of 25 mm-diameter milled voids with different heights located in triple-slab SOFI panel at substrate obtained using the 6 mm-diameter footprint lens antenna.

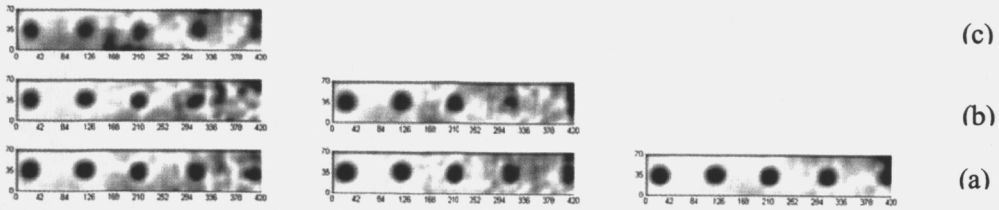

Figure 11: Processed 100 GHz images of 25 mm-diameter milled voids with different heights located in SOFI panels at different depths: (a) at substrate, (b) 70 mm from substrate and (c) 140 mm from substrate.

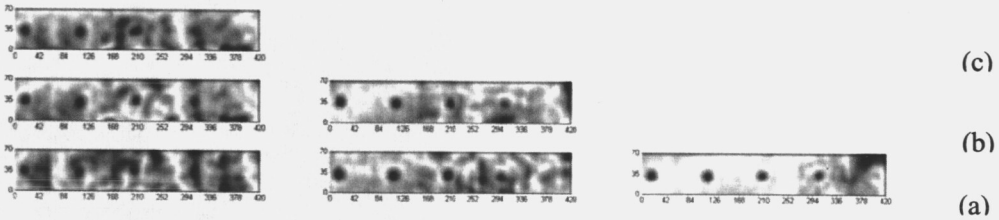

Figure 12: Processed 100 GHz images of 6 mm-diameter milled voids with different heights located in SOFI panels at different depths: (a) at substrate, (b) 70 mm from substrate and (c) 140 mm from substrate.